CLEAN beamforming for the enhanced detection of multiple infrasonic sources

den Ouden, Olivier; Assink, Jelle D.; Smets, P.S.M.; Shani-Kadmiel, Shahar; Averbuch, Gil; Evers, Läslo

DOI
10.1093/gji/ggaa010

Publication date
2020

Document Version
Final published version

Published in
Geophysical Journal International

Citation (APA)
den Ouden, O., Assink, J. D., Smets, P. S. M., Shani-Kadmiel, S., Averbuch, G., & Evers, L. (2020). CLEAN beamforming for the enhanced detection of multiple infrasonic sources. *Geophysical Journal International*, *221*(1), 305-317. https://doi.org/10.1093/gji/ggaa010

Geophysical Journal International

Geophys. J. Int. (2020) **221,** 305–317
Advance Access publication 2020 January 8
GJI General Geophysical Methods

doi: 10.1093/gji/ggaa010

CLEAN beamforming for the enhanced detection of multiple infrasonic sources

Olivier F.C. den Ouden [1,2] Jelle D. Assink,[1] Pieter S.M. Smets [1,2]
Shahar Shani-Kadmiel,[2] Gil Averbuch[2] and Läslo G. Evers [1,2]

[1] *R&D Department of Seismology and Acoustics, Royal Netherlands Meteorological Institute,* 3730 *AE De Bilt, The Netherlands.*
E-mail: olivier.den.ouden@knmi.com
[2] *Department of Geoscience and Engineering, Delft University of Technology,* 2628 *CN Delft, The Netherlands*

Accepted 2020 January 6. Received 2020 January 6; in original form 2019 July 8

SUMMARY

The detection and characterization of signals of interest in the presence of (in)coherent ambient noise is central to the analysis of infrasound array data. Microbaroms have an extended source region and a dynamical character. From the perspective of an infrasound array, these coherent noise sources appear as interfering signals that conventional beamform methods may not correctly resolve. This limits the ability of an infrasound array to dissect the incoming wavefield into individual components. In this paper, this problem will be addressed by proposing a high-resolution beamform technique in combination with the CLEAN algorithm. CLEAN iteratively selects the maximum of the *f*/*k* spectrum (i.e. following the Bartlett or the Capon method) and removes a percentage of the corresponding signal from the cross-spectral density matrix. In this procedure, the array response is deconvolved from the *f*/*k* spectral density function. The spectral peaks are retained in a 'clean' spectrum. A data-driven stopping criterion for CLEAN is proposed, which relies on the framework of Fisher statistics. This allows the construction of an automated algorithm that continuously extracts coherent energy until the point is reached that only incoherent noise is left in the data. CLEAN is tested on a synthetic data set and is applied to data from multiple International Monitoring System infrasound arrays. The results show that the proposed method allows for the identification of multiple microbarom source regions in the Northern Atlantic that would have remained unidentified if conventional methods had been applied.

Key words: Atlantic Ocean; Spatial analysis; Time-series analysis.

1 INTRODUCTION

Sensor arrays are used in various geophysical disciplines for a detailed study of signals that are part of a complex wavefield. The use of arrays allows for an enhanced detection of signals in the presence of incoherent noise, as the signal-to-noise ratio (SNR) is improved by summation across the array elements. In addition, arrays can be used to estimate the directivity of incoming wave fronts, and therefore can be used as spatial filters by steering the array towards the direction of interest. This has led to applications in the fields of seismology (Harjes & Henger 1973; Husebye & Ruud 1989; Schweitzer *et al.* 2002), acoustics (Billingsley & Kinns 1976; Michel *et al.* 2006) and astronomy (Jansky 1932; Garrett 2013).

In this article, array detection of inaudible low-frequency sound, or infrasound, is discussed. The detection of infrasonic sources over long distances depends on the spectral content of the source, the atmospheric propagation conditions along the source–receiver path, as well as the local noise conditions near the array. The vertical temperature and wind structures determine the propagation paths while absorption affects the amplitude and frequency contents of the received signal (Waxler & Assink 2019). Because attenuation is strongly dependent on the acoustic frequency, lower frequency signals can propagate over significantly longer distances when compared to higher frequencies (Sutherland & Bass 2004). The local noise conditions are determined by the turbulent motions in the atmospheric boundary layer, near the array (Smink *et al.* 2018).

The International Monitoring System (IMS) is in place for the verification of the Comprehensive Nuclear-Test-Ban Treaty (CTBT) and monitors the atmosphere globally for infrasonic signals from nuclear tests, using microbarometer arrays. Currently, 51 out of 60 microbarometer arrays provide real-time infrasound recordings from around the world. The IMS has played a central role in the characterization of the global infrasonic wavefield and the localization of infrasound sources, which include earthquakes, lightning, meteors, (nuclear) explosions, colliding ocean wave–wave and surf (Campus & Christie 2010). The infrasonic wavefield is complex

and often consists of interfering acoustic signals in overlapping frequency bands, in the presence of incoherent noise. The acoustic signals take the form of transients, (quasi-)continuous signals or a combination of both. From the perspective of an array, coherent noise sources appear as interfering signals that clutter the array detection bulletins and may obscure detections from signals of interest.

Most infrasound processing routines, including those that are used for real-time processing of the IMS infrasound arrays, are designed to only detect the dominant acoustic signal in a given time segment and frequency band. However, various beamform techniques exist in the literature that allow for the detection of signals from multiple spatially distributed sources (Viberg & Krim 1997; Rost & Thomas 2002). The capability of detecting and classifying interfering sources relies on the beamform resolution as quantified by the array response, which is determined by the beamform technique and the array layout. A low beamform resolution could lead to the dominant source masking subdominant sources.

In this study, the CLEAN algorithm (Högbom 1974) is applied for high-resolution array processing of infrasound data. CLEAN is a post-processing method that iteratively selects the main contribution in the *f*/*k* spectrum and removes a percentage of the corresponding signal from the cross-spectral density matrix. In this procedure, the array response is deconvolved from the resolved *f*/*k* spectral density function. The spectral peaks are retained in a 'clean' spectrum. This iterative process continues until a stopping criterion is reached. The beamform techniques proposed by Bartlett (1948) and Capon (1969) can be used to compute the *f*/*k* spectrum. Previous studies (Clark 1980; Sijtsma 2007; Gal *et al.* 2016), have shown that the application of CLEAN provides a superior beamform resolution. Moreover, it has been shown that the performance critically depends on the setting of two parameters: the percentage of removal and the stopping criterion. In this work, the use of Fisher statistics is proposed and applied as stopping criterion for the iterative CLEAN procedure. This statistical framework has been established for significance testing of multivariate data (Fisher 1948), and has applications in geophysical signal processing (Melton & Bailey 1957; Shumway 1971; Smart & Flinn 1971).

The remainder of this article is organized as follows. Section 2 introduces the beamform techniques, CLEAN as post-processing method and the proposed CLEAN parametrization. The performance of CLEAN, as tested using synthetic data, is presented in Section 3. In Section 4, CLEAN is applied to IMS infrasound array data and it demonstrates that multiple microbarom source regions can be resolved in the Northern Atlantic. Finally, the results are discussed and summarized in Section 5.

2 DESCRIPTION OF THE ALGORITHM

2.1 Frequency-domain beamforming

Consider an array of N omnidirectional receivers, with $N \geq 3$ (Fig. 1). Each array element has position $r_{n,\ldots,N} = (x_n, y_n, z_n)$, of which the absolute value is the distance between the element and a reference distance, for example, the geometrical centre of the array. Often an array exists of elements close to the geometrical centre to resolve the high frequencies of the wave front, and elements that lie further away to resolve the low frequencies. In the case of interest, it is assumed that the array is situated in the far-field. Therefore, the wavefield can be represented as a superposition of 3-D planar wave fronts, propagating with phase speed c. The goal is to estimate the 3-D wave-front parameters as a function of time t and frequency f. For this purpose, it is useful to consider a plane-wave decomposition of the incoming wavefield, in terms of a frequency–wavenumber (f/k) spectral density $G(f, \vec{k})$:

$$G(f,\vec{k}) = \int_{-\infty}^{\infty}\int_{-\infty}^{\infty}\int_{-\infty}^{\infty} G(f,\vec{r})\mathrm{e}^{i(\vec{k}\cdot\vec{r})}\mathrm{dx\ dy\ dz}, \tag{1}$$

here, $\vec{k} = (k_x, k_y, k_z)$ and $G(f, \vec{r})$ represent the 3-D wavenumber vector and the Fourier transformed array recordings, respectively. Beamforming can be used to separate the coherent and incoherent parts of $G(f, \vec{k})$.

Most infrasound arrays are ground-based planar arrays (Edwards & Green 2012), in which case the integral in eq. (1) can be reduced to a two-dimensional integral over x and y. This also implies that only the horizontal component of $\vec{k}$ can be directly estimated in the beamforming process. The vertical component, k_z, is typically inferred through the dispersion relation, $|\vec{k}| = 2\pi f/c$ and an estimate of the phase speed c, that is, the speed of sound near the array. The wavenumber vector $\vec{k}$ can be expressed in terms of a slowness vector $\vec{p}$ by scaling with the angular frequency, $\omega = 2\pi f$. The horizontal component of $\vec{p}$ can be related to the apparent velocity c_{app} and backazimuth θ as follows:

$$c_{\mathrm{app}} = \frac{1}{|\vec{p}_{x,y}|} \qquad \theta = \arctan\frac{p_x}{p_y}.$$

The apparent velocity corresponds to the horizontal propagation speed of a wave front, that is, as would be measured by the ground-based array. The backazimuth relates to the horizontal incidence angle, with respect to the north.

To beamform the array data, a cross-spectral density matrix $C(f)$ is to be estimated:

$$C(f) = \frac{1}{L}\sum_{l=1}^{L} G_l(f,\vec{r})G_l^*(f,\vec{r}), \tag{2}$$

here, $*$ denotes the conjugate transpose. The off-diagonal elements of matrix $C(f)$ contain the phase delays between each sensor pair, while the diagonal elements contain the power spectral density of each element. It is common to estimate the cross-spectral density matrix $C(f)$ by averaging over L snapshots within one single time window of waveform data, $G_l(f, \vec{r})$. The averaging using snapshots is crucial for the application of Capon's method (Capon 1969), as the beamform weights rely on the matrix inverse of $C(f)$. To ensure that the inverse exists, $C(f)$ must be full-rank and therefore L needs to be sufficiently large, that is, $L \geq N$ (Viberg & Krim 1997). Assuming that the mathematical representation of the signal of interest and noise are statistically independent, the cross-spectral density matrix can be factored into a signal and noise co-variance matrix:

$$C(f) = E\{GG^*\} = E\{G_sG_s^*\} + E\{G_uG_u^*\}, \tag{3}$$

where $E\{\}$ indicates the statistical expectation, $E\{G_sG_s^*\}$ indicates the signal co-variance matrix and $E\{G_uG_u^*\}$ the noise co-variance matrix. Noise has a common variance σ^2 and is assumed to be uncorrelated between all sensors. This decomposition is useful in the development of the CLEAN stopping criterion as will be discussed in Section 2.3.

With the definition of $C(f)$, the f/k spectrum $P(f, \vec{k})$ can be computed by multiplying with beamform weight factor $w(\vec{k})$:

$$P(f,\vec{k}) = w^*(\vec{k})C(f)w(\vec{k}). \tag{4}$$

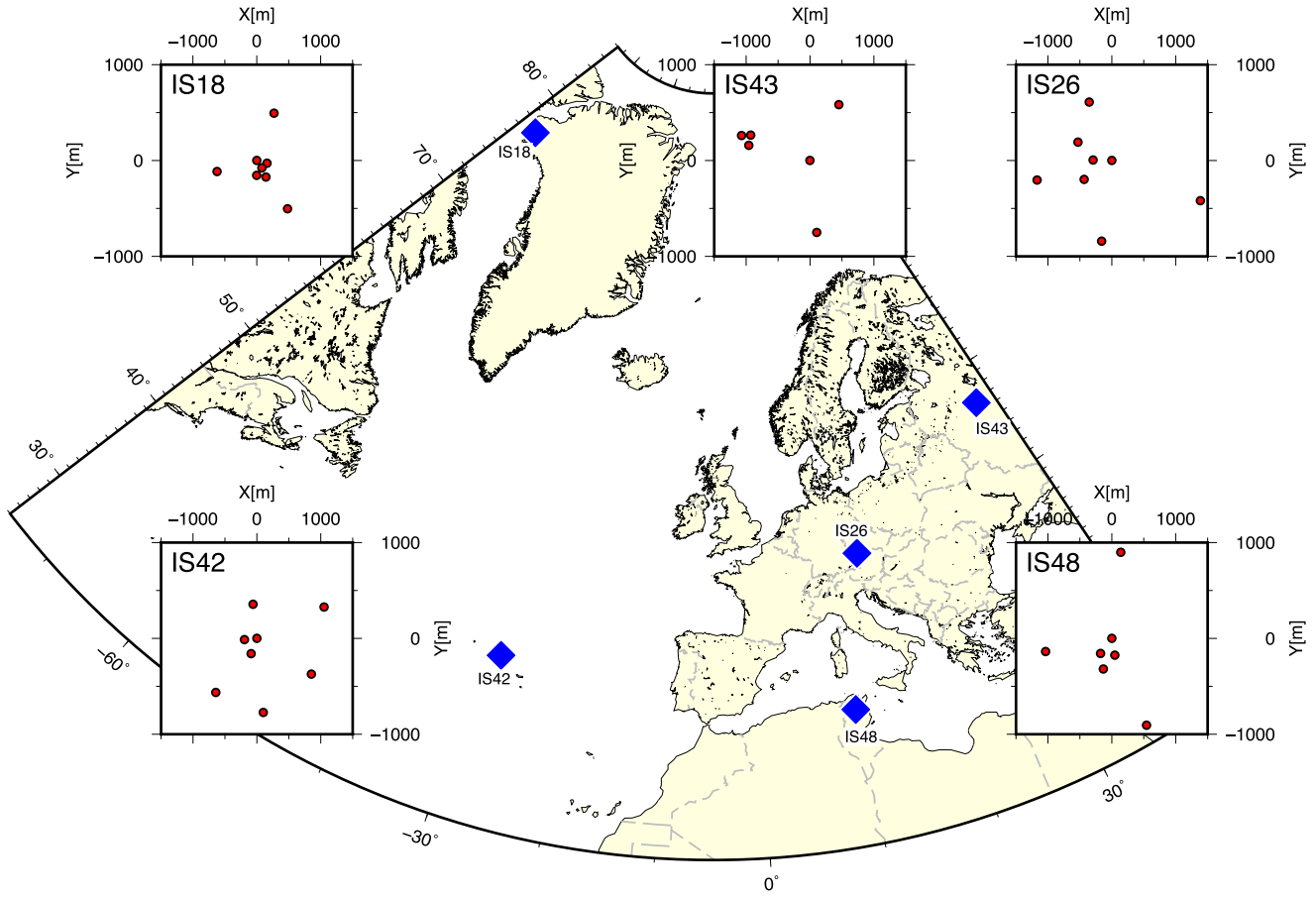

Figure 1. Array locations and layouts of IS18, IS26, IS42, IS43 and IS48.

This formulation allows for the comparison of various beamform weights. In this paper, the Bartlett and Capon weights and corresponding *f*/*k* spectra are compared. For the Bartlett, or 'classical' *f*/*k* spectrum, the signal power in $P(f, \vec{k})$ is maximized by summing the phase-aligned spectral values. The Bartlett weight $w_B(\vec{k})$ has been derived as

$$w_B(\vec{k}) = \frac{a(\vec{k})}{\sqrt{a^*(\vec{k})a(\vec{k})}}, \tag{5}$$

where $a(\vec{k}) = \mathrm{e}^{-i(\vec{k}\cdot\vec{r})}$ represents the steering vector. The calculation of the *f*/*k* spectra occurs over a vector space spanned by those steering vectors, which is dependent on the used slowness grid. Fig. 2 shows the design of the slowness grid, which consists of a 360° ring grid plus a rectangular grid. The ring grid is a linear grid in backazimuth and apparent velocity, ranging from 0° to 360° and 285 to 500 m s^{-1} with steps of 1° and 1 m s^{-1}, respectively. This ring grid is, however, nonlinear in the slowness domain. The rectangular grid consists of linearly spaced values between −0.005 and 0.005 s m^{-1}. This grid is added to ensure that energy from outside the ring grid does not clutter on its boundaries, which would result in biased outcomes.

Capon's method is derived as a maximum likelihood filter. The filter design is determined by the inverse of cross spectral density matrix $C(f)$ and steering vector $a(\vec{k})$. With this design, the noise in the power spectrum is optimally suppressed while keeping a constant gain in the direction of interest. For Capon's method, $w_C(\vec{k})$

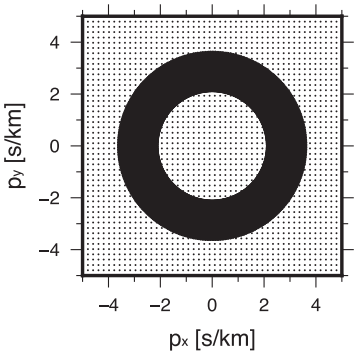

Figure 2. The applied slowness grid, consisting of a 360° ring grid (between 275 and 475 m s^{-1} with steps of 1 m s^{-1} every 1°), and a 2500-point equidistant squared grid (between 200 and 10 000 m s^{-1}).

has been derived as

$$w_C(\vec{k}) = \frac{C^{-1}(f)a(\vec{k})}{a^*(\vec{k})C^{-1}(f)a(\vec{k})}. \tag{6}$$

To study the spectral properties of these beamform techniques, it is instructive to evaluate the array response. It is defined as the *f*/*k* spectrum $P(f, \vec{k})$ for a monochromatic wave with unit amplitude or $G(f_0, \vec{k}_0) = (1/N) \cdot \mathrm{e}^{i\vec{k}_0\cdot\vec{r}}$, for which $k_0 = 2\pi f_0/c$. The array response function may consist of several maxima. The absolute maximum is found at $\vec{k} = \vec{k}_0$ and corresponds to the main lobe. Several side lobes may appear that are a consequence of the spatial sampling of the wavefield with a discrete number of array elements. A higher

resolution array, for example, better peaked absolute maximum, can be obtained by modifying the locations of the array elements or by adding elements to the array. (Evers 2008).

Fig. 3 shows the Bartlett and Capon array responses for IMS Infrasound array IS48, for a monochromatic wave with $f_0 = 0.3$ Hz and $k_0 = 0$ m^{-1}. The array layout of IS48 is shown in Fig. 1. Capon's array response has a much sharper main lobe when compared to Bartlett's response, which reflects its well-known high spatial resolution property. Moreover, it can be noted that the side lobes in Capon's spectrum are significantly reduced, when compared to Bartlett's response. This gain in resolution comes at a computational cost, because of the matrix inversion of $C(f)$. In addition, some temporal resolution (e.g. transient signals) is lost because of the necessary averaging process, as described by eq. (2). When using Bartlett it is harder to distinguish between two closely located sources in the f/k spectrum, due to resolution. This favours the use of Bartlett's method for the analysis of transient signals, as it merits higher temporal resolution analyses. Whereas Capon's method is more suited for the analysis of (quasi-)continuous signals with longer time windows, such as microbaroms.

2.2 CLEAN

In the processing of real data, the f/k spectrum often consists of multiple maxima with varying amplitude. In such a convoluted spectrum, it can be difficult to distinguish interfering sources and identify concurrent, subdominant sources from the side lobe of a dominant source. It is the objective here, to design a method that can unravel the f/k spectrum in terms of individual contributions to the f/k spectrum, while being able to distinguish between main lobe and side lobes. For this purpose, the CLEAN method can be applied.

CLEAN (Högbom 1974) is a post-processing method that can be applied to conventional beamform methods, for example, Bartlett and Capon as introduced in the previous subsection. CLEAN iteratively removes phase and amplitude information associated with the strongest contribution in the f/k spectrum, $P_{\max}$, from the cross-spectral density matrix (Sijtsma 2007; Gal *et al.* 2016). A partly cleaned cross-spectral density matrix, C_{clean}, is obtained:

$$C^{j+1}_{\text{clean}}(f) = C^{j}_{\text{clean}}(f) - \phi P^{j}_{\max} w_{\max} w^{*}_{\max}, \tag{7}$$

with $w_{\max} = w(k_{\max})$ the beamform weight for which $P_{\max}$, with wavenumber $k_{\max}$, was resolved, C^{j}_{clean} the cross-spectral density matrix at j_{th} iteration and ϕ the parameter that determines the fraction of removed power. Note that the subtraction in eq. (7) involves a convolution of the array response function with $P_{\max}$. This ensures that the array response pattern is suppressed in the $(j+1)_{\text{th}}$ beamform iteration, following eq. (4). It is precisely this deconvolution operation that allows for the identification of subdominant f/k spectral density peaks. Such peaks could otherwise have been masked due to spatial aliasing of the dominant source in the beamforming process.

The CLEAN algorithm has a relatively high computational cost because of the potentially large number of beamform iterations in lieu of one single beamforming run. The number of iterations is controlled by the ϕ value. A small value will result in resolving more subdominant sources at the cost of a larger number of iterations and therefore a higher computational load, while a larger value leads to a faster algorithm but may be less accurate in resolving subdominant sources. Gal *et al.* (2016) stated that the optimal value for ϕ depends on the combination of array layout, frequency range of beamforming and the SNR. In general, a small ϕ value is recommended when processing data from arrays with a small number of elements and/or data with low SNR values.

In this study, the number of iterations is not pre-defined but depends on a stopping criteria (Section 2.3). CLEAN beamforming with ϕ values between 5 and 15% provided similar results. Since this study deals with a low number of array elements and a low SNR, a ϕ value of 10 per cent has been chosen (following Gal *et al.* 2016).

For each processed frequency f, the maximum of the f/k spectral density as well as the corresponding wavenumber vector $\vec{k}_j$ is stored in a CLEAN power spectrum:

$$P_{\text{clean}}(f, \vec{k}) = \sum_{j}^{Q} \phi P^{j}_{\max}(f, \vec{k}_j), \tag{8}$$

where Q is the total number of CLEAN iterations. The CLEAN process continues until reaching a stopping criterion. Because the array response function is deconvolved, the smearing of energy in the original f/k power spectrum $P(f, \vec{k})$ has been reduced. As a result, $P_{\text{clean}}(f, \vec{k})$ has a sharper and cleaner appearance, which is useful in obtaining an enhanced insight in the diversity of acoustic sources around the array.

The individual contributions $P^{j}_{\max}(f, \vec{k}_j)$ in $P_{\text{clean}}(f, \vec{k})$ are characterized by a new and clean, Gaussian point spread function (PSF; Sijtsma 2007). Every PSF has a standard deviation of three times the spatial f/k spectral resolution. Hence, sources are distinct if the distance between the maxima of two PSFs is greater than two standard deviations.

2.3 Fisher statistics as CLEAN stopping criterion

As CLEAN is an iterative beamforming procedure, a maximum number of iterations is to be defined after which the procedure stops. Hitherto, setting of this parameter has been user defined (Clark 1980; Sijtsma 2007; Gal *et al.* 2016), which is impractical for application to large data sets, for which the number of iterations may be strongly dependent on the analysis window. Here, the use of Fisher statistics and the F-ratio a test statistic (Fisher 1948) is proposed for the definition of a data-driven stopping criterion.

The processing of data from a ground-based infrasound array corresponds to a bi-variate analysis problem where the pressure fluctuations are modelled as a random process. Within each analysis window, the variance of the (phase-shifted) pressure signals between the array elements is compared with the variance of the pressure values at each individual element (Melton & Bailey 1957). The F-ratio compares both measures of variance. In the associated statistical test, the null hypothesis is tested that these variances are not significantly different. In other words: the null hypothesis corresponds to the case that no coherent signal is present. The F-ratio deviates from unity if the variances are not equal, which corresponds to a probability that a coherent signal is present in the data. Fisher's test statistic is evaluated for every steering vector that is considered in the beamforming procedure. This procedure allows an evaluation of the significance of detection on each steering vector of interest.

The probability density of the F-ratio is described by an F-distribution. The particular shape of the distribution is dependent on the statistics of the data samples as well as the degrees of freedom of the data set. In the beamform application, the degrees of freedom are a function of the number of samples points T and array elements N. If the samples points follow the statistical distribution of Gaussian white noise, the resulting F-ratio statistic follows a central

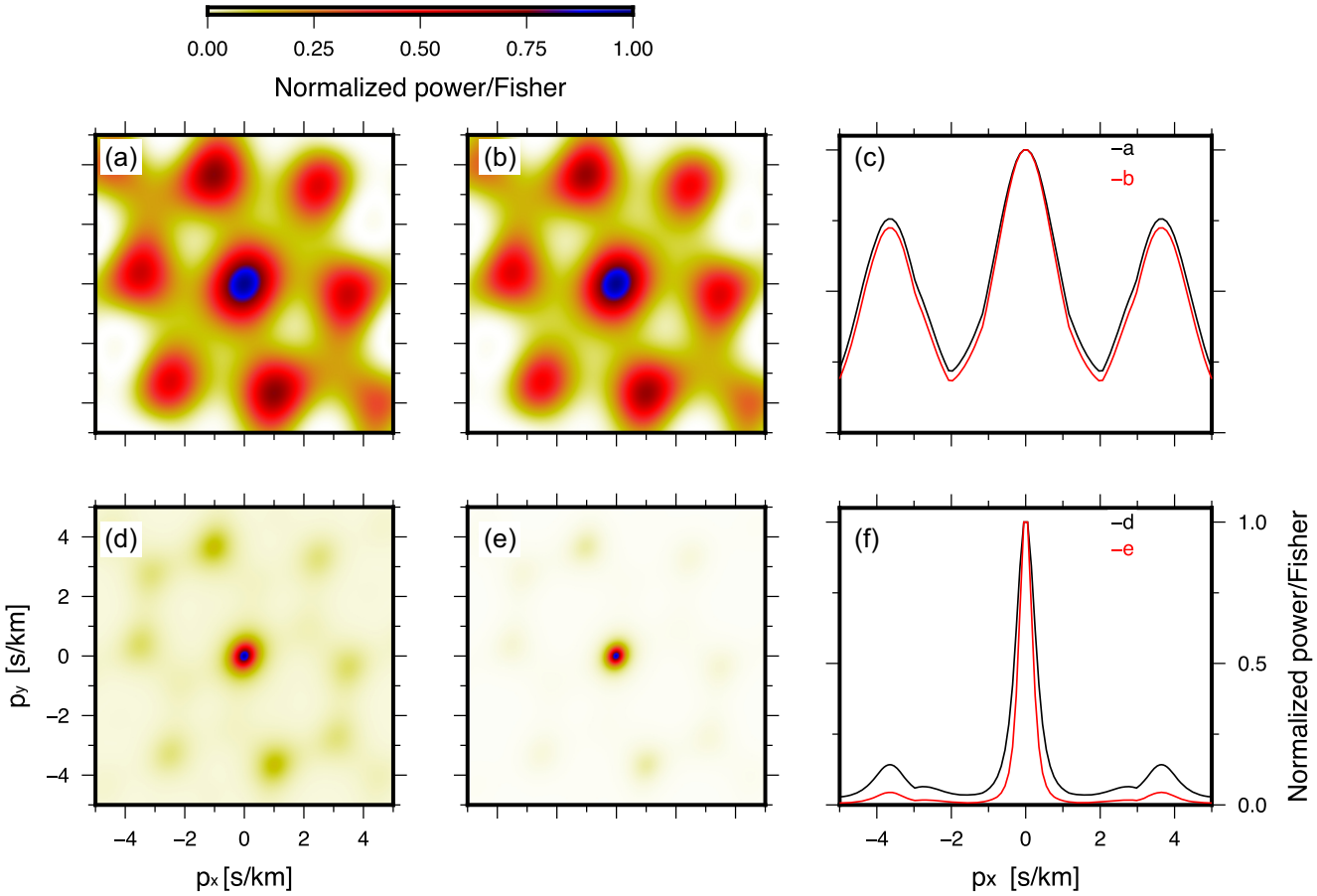

Figure 3. Array response of infrasound array IS48 at 0.3 Hz, following the Bartlett (a) and Capon (d) beams. The array response improves after applying the Fisher statistics for Bartlett (b) as well Capon (e). The side spectra (c and f) show the improvement of the Fisher ratio (red curve) with respect to the array response in terms of normalized power (black curve) at $p_y = 0$.

F-distribution $F(\nu_1, \nu_2)$. The degrees of freedom in the time-domain Fisher analysis, ν_1 and ν_2, are given by $\nu_1 = T_t - 1$ and $\nu_2 = T_t(N - 1)$ (Evers 2008). In the frequency domain, the degrees of freedom are given by: $\nu_1 = 2T_f$ and $\nu_2 = 2T_f(N - 1)$ (Shumway 1971). The mean of the central distribution is $F = 1$. The F-ratio statistic follows a non-central F-distribution $F(\nu_1, \nu_2, \lambda_{nc})$ in the case where a signal with a certain SNR is present. The non-centrality parameter λ_{nc} is determined by the SNR of the signal as: $\lambda_{nc} = \nu_1 \cdot \mathrm{SNR}^2$ (Shumway 1971).

The statistical properties of the F-ratio allow for the estimation of the missed event and false alarm probabilities, given a specified confidence level. Likewise, a probability of detection can also be quantified. Therefore, the Fisher's test statistic is a robust and efficient method for the detection of coherent signals in the presence of incoherent noise. Besides, representing the spectra in terms of the F-ratio sharpens the main lobes, as can also be seen in Fig. 3.

The relation between the F-ratio and the SNR has been derived by Melton & Bailey (1957).

$$F = N \cdot \mathrm{SNR}^2 + 1. \tag{9}$$

In the derivation of this relation, it is assumed that the signal is identical over all array elements while the noise can be modelled as uncorrelated Gaussian white noise. Smart & Flinn (1971) have shown that the F-ratio in the frequency domain can be defined using the following estimates of signal power on the beam $P_{\max}$, and total power P_t:

$$F(f, \vec{k}) = \frac{P_{\max}(f, \vec{k})}{P_t(f) - P_{\max}(f, \vec{k})}(N - 1). \tag{10}$$

Here, $P_t(f)$ represents the total f/k spectral power as a normalized sum of the diagonal elements of the cross-spectral density matrix:

$$P_t(f) = \frac{1}{N}\sum_{n=1}^{N} C_{nn}(f). \tag{11}$$

By evaluating the Fisher ratio at every CLEAN iteration, the probability of detection and the SNR of the detected signal can be estimated. Moreover, this framework allows us to determine a CLEAN stopping criterion from a statistical perspective. Indeed, as the Fisher ratio approaches unity, the likelihood of a false alarm increases and the iterative procedure can be stopped, as no coherent signal is likely to be left in the cross-spectral density matrix. The effectiveness of this method will be demonstrated using synthetic data in the following section.

3 SYNTHETIC DATA

Three different synthetic waveform tests are discussed in this section. The tests have been designed to (1) evaluate the use of Fisher statistics as a CLEAN stopping criterion, (2) compare the Bartlett and Capon beamform techniques and (3) evaluate the performance

of the proposed CLEAN algorithm in the processing of infrasound array data. The synthetic waveforms are generated given the array element locations of infrasound array IS48 (Fig. 1). The temporal sample rate of the waveforms is 20 Hz, which corresponds to the actual sample rate of this IMS array.

3.1 Fisher threshold testing using uncorrelated Gaussian white noise

To demonstrate the use of Fisher statistics in the determination of a CLEAN stopping criterion, a Monte Carlo simulation is performed. The Monte Carlo simulation consists of 500 Capon beamform runs on synthetic waveform data that consists of uniform Gaussian white noise. The beam forming analysis is carried out in the frequency band ranging from 0.1 to 0.3 Hz. Smoothing is applied by averaging power estimates for Z adjacent frequencies around a frequency of interest, which is defined by the amount of steps within the frequency band. To satisfy the degrees of freedom in the time domain and the frequency domain, smoothing should avoid overlapping frequencies. For each run, each with a duration of 1000 s, data are beamformed. The Fisher ratio is computed for every beam. Fig. 4(a) shows an example f/k spectrum.

The resulting distribution of calculated Fisher ratios is plotted in Fig. 4(b) as a histogram. The histogram distribution follows a central F-distribution, which would be expected as the data samples follow the statistical distribution of Gaussian white noise. The F-distribution is characterized by the degrees of freedom which are specified by $N = 7$ and $T_f = Z + L = 10 + 40 = 50$, which indicates the number of sample points that are used, depending on the smoothing and the number of snapshots, L, within one window. The distribution is plotted with a solid black line in Fig. 4(b). The 95 percentile is found at $F = 1.28$ and is indicated by the dotted line. For this particular choice of processing parameters, the Fisher threshold should be set to 1.28 in order to have a 95% confidence for avoiding false-alarms. More generally, this test demonstrates the use of Fisher statistics in the estimation of a CLEAN stopping criterion.

3.2 Slowness estimates for multiple, interfering sources of coherent noise

Two additional synthetic data sets are constructed in order to test the ability to accurately discriminate between interfering sources within one analysis window. The synthetic waveforms are generated for each of the array elements, by adding Gaussian white noise with a specified amplitude as described in Table 1. The synthetic waveforms for each element are coherent, but shifted in time with respect to one another, according to the array layout and the imposed directivity of signal m. Each source is continuous, to represent ambient noise. Table 1 shows the characteristics of data set A. The applied bandpass filter has corner frequencies of 0.1 and 0.3 Hz. Note that the three sources are continuously interfering throughout the record.

The time-shift for each array element is computed using the steering vector $a(\vec{k}_m)$ and wavenumber vector parameters:

$$k_{x,m} = \frac{2\pi f}{c_{\mathrm{app},m}} \sin(\theta_m) \qquad k_{y,m} = \frac{2\pi f}{c_{\mathrm{app},m}} \cos(\theta_m).$$

The individual signal contributions are added up per element, thereby generating a complex signal that is composed of several individual signals. Finally, uncorrelated Gaussian white noise with amplitude 0.5 Pa is added to each of the array element waveforms, individually. As this signal is incoherent between the array elements, it represents the noise level. Hence, a theoretical signal-to-noise power ratio and Fisher ratio can be estimated from eq. (9).

Fig. 5 shows the initial f/k spectra before and after application of CLEAN. Three features should be noted. First, CLEAN improves the resolution of both spectra, as can be seen in the sharpening of the main lobes. This enables to resolve two closely located sources within the f/k spectrum. The highest resolution is obtained by combining Capon and CLEAN. Gal *et al.* (2016) earlier stated that a high-resolution initial f/k spectrum with a sharp main lobe is beneficial to the performance of CLEAN. Second, with Capon the sources are better identified than with Bartlett, as can be seen from the coincidence of the lobes with the circles, which have their centre points at the expected source locations and a radius of $\pm 1.5^\circ$. This is a consequence of the lower resolution of Bartlett. Last, the low spatial resolution of Bartlett leads to various spurious peaks in the f/k spectrum, after application of CLEAN.

The θ_m and c_{app} parameters that correspond to the maxima of the resolved f/k spectral densities after CLEAN has been applied are tabulated in Table 1. In case of Capon in combination with CLEAN, a close agreement between the source parameters and the resolved values is noted. This is not the case when applying Bartlett's method, due to the low resolution of the initial f/k spectra.

While a particularly good agreement is noted for the backazimuth and the resolved apparent velocity in case of Capon and CLEAN, the resolved Fisher ratio is biased low compared to the theoretical Fisher ratio, which will be further explained in the discussion.

Based on the comparative performance of the beamform techniques, the last synthetic test is performed with Capon's method only.

The parameters used in the construction of data set B are summarized in Table 2. Data set B represents the case of an increasing number of interfering, continuous sources with time. The synthesis of the signals is otherwise equal to the method described earlier in this section. Fig. 6 shows the f/k spectra and the resulting θ_m and c_{app} as function of time. The circles indicate the expected source positions and the colour rings indicates the expected apparent velocity of the signals. Again, a close agreement between the source parameters and the resolved values is noted. The numerical values are summarized in Table 2.

Since the input and output of both data sets are in good agreement, we conclude that the proposed Fisher ratio as a stopping criterion and the PSF in combination with the two standard deviation distribution are robust parameters. Both enable CLEAN to be data-driven and reliable.

4 REAL DATA EXAMPLE

The proposed CLEAN method is applied to infrasound measurements recorded on 2011 January 17 on the IMS infrasound arrays IS48 (Tunisia), IS42 (Açores), IS26 (Germany), IS43 (Russia) and IS18 (Greenland).

This analysis builds on an earlier study by Assink *et al.* (2014) in which two simultaneous infrasound sources were identified in the microbarom frequency band using a beamform technique using Bartlett's method and Fisher statistics. It was hypothesized that the detections corresponded to microbarom activity in the Northern Atlantic and Mediterranean Sea.

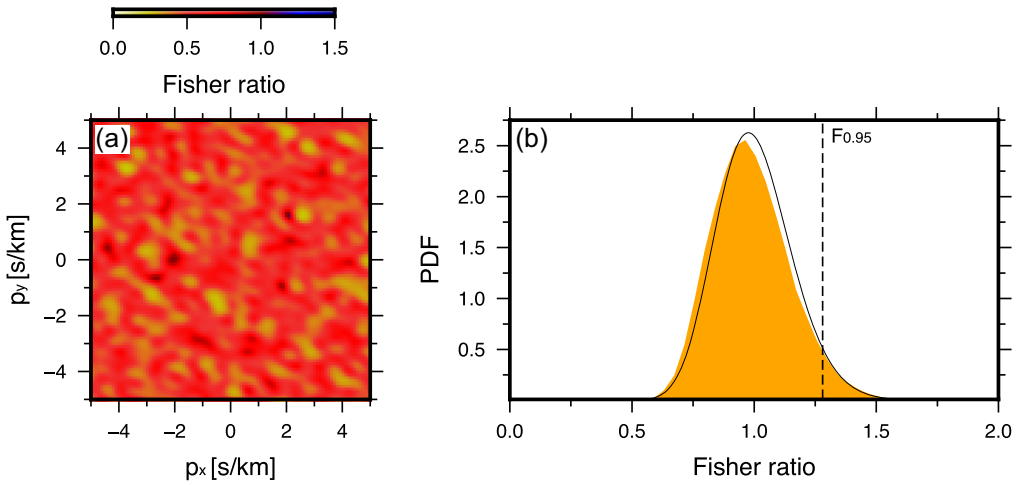

Figure 4. Outcome of the Monte Carlo runs on randomly generated data. (a) The *f*/*k* beamforming result of a randomly generated data set. (b) Histogram F-ratio outcome of 500 Monte Carlo runs. The grey line indicates the central F-distribution. The dotted line is the 95 percentile, $F_{0.95} = 1.28$.

Table 1. Input source parameters for data set A and its estimated parameters using the CLEAN algorithm, following Bartlett's and Capon's method. The amplitude of the added incoherent white noise is 0.5 Pa. The expected F-ratio is computed using eq. (9).

Input				Output Bartlett			Output Capon		
θ_m	$c_{\text{app},\,m}$ (m s^{-1})	s_m (Pa)	Exp. F-ratio	θ_m	c_{app} (m s^{-1})	F-ratio	θ_m	c_{app} (m s^{-1})	F-ratio
300	340	1.0	29	294	335	28	300	339	27
90	340	0.8	19	93	330	14	90	340	20
280	340	0.6	11	277	324	7	280	338	7

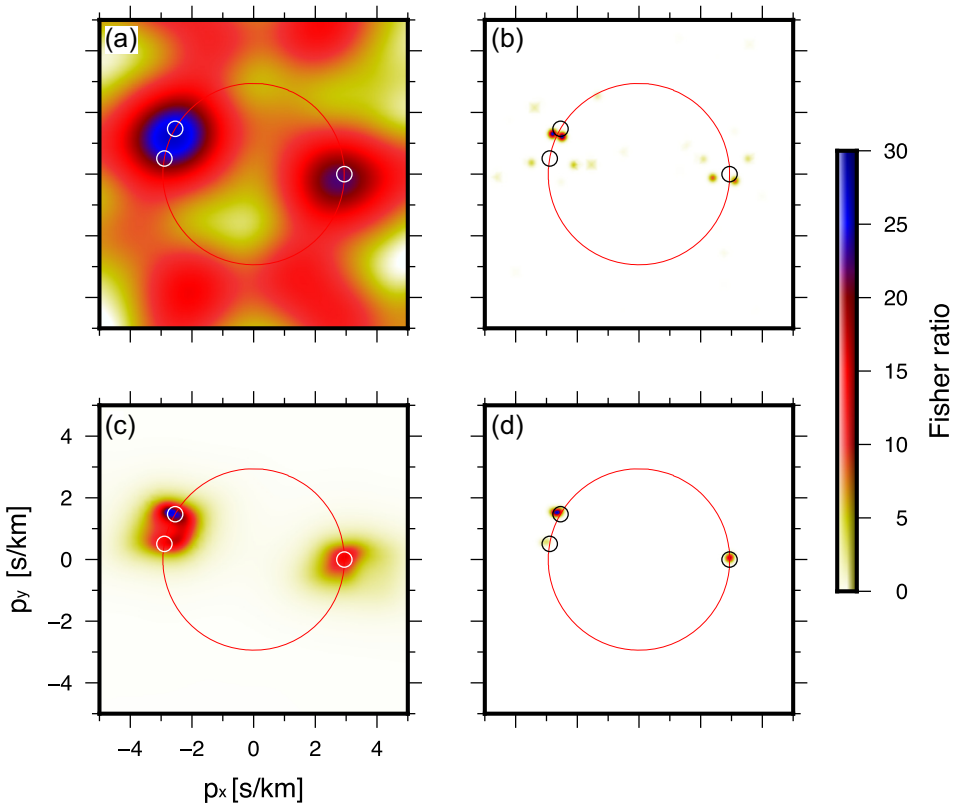

Figure 5. Beamform results of IS48 between 0.1 and 0.3 Hz on synthetic data set A (Table 1). Panels (a) and (b) show the results of the Bartlett beamformer before and after CLEAN has been applied. Panels (c) and (d) show the results when Capon has been applied. The circles indicate where sources are expected in the *f*/*k* spectrum. The red ring indicates the apparent velocity, $c_{\text{app}} = 340$ m s^{-1}. Note that the apparent sources in frame (b) correspond to side-lobes due to Bartlett's method.

Table 2. Similar as Table I, but now for data set B, which features three different sources that are active during different time intervals. In this case, the CLEAN method is used with Capon's method, only.

Input					Output		
θ_m	c_{app} (m s^{-1})	s_m (Pa)	Exp. F-ratio	Time (s)	θ_m	c_{app} (m s^{-1})	F-ratio
300	360	1.0	29	100–4000	300	359	28
90	320	0.8	19	1100–4000	89.8	319	17
280	280	0.6	11	2100–4000	279.6	278	9

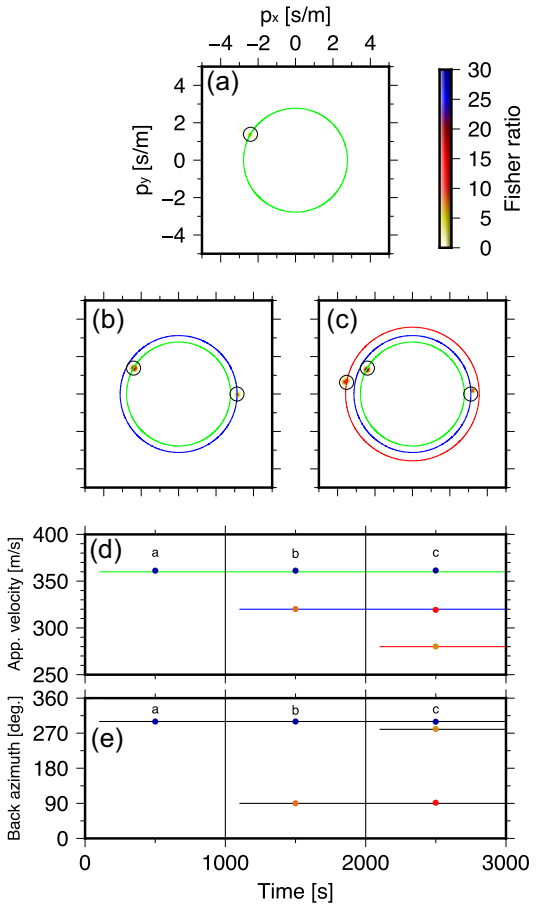

Figure 6. Result of Capon beamforming with CLEAN on waveforms of data set B, Table 1. The *f*/*k* spectra of window 1 (a), window 2 (b) and window 3 (c) after CLEAN has been applied. The circles indicate where sources are expected, and the coloured rings indicate the apparent velocity c_{app} (green, c_{app} = 360 m s^{-1}; blue, c_{app} = 320 m s^{-1}; and red, c_{app} = 280m s^{-1}). Panels (d)–(e) show the CLEAN results plotted as a function of time, for the three windows considered. The lines indicate expected results regarding backazimuth and apparent velocity, colour of the dots indicates the Fisher ratio.

The two sources had an overlapping frequency content around 0.2 Hz, but the Mediterranean microbaroms were found to be coherent up to 0.6 Hz while the North Atlantic microbaroms are coherent up to 0.3 Hz.

Fig. 7 shows the *f*/*k* spectra of the IMS arrays for the first 2000 s of data on 2011 January 17, before and after CLEAN has been applied and by using the 95 percentile Fisher threshold (Section 3.1). In these spectra, multiple sources are resolved in the 0.1–0.3 Hz frequency band. It should be noted that subdominant sources can be identified, which would have been obscured in traditional infrasound processing schemes that only report on the dominant source. Fig. 8 shows the processing results of IS48 for the entire day. Figs 8(a) and (b) show the dominant source per time window, using Bartlett's and Capon's method, respectively. Fig. 8(c) lists all the resolved sources by using Capon in combination with CLEAN. The conventional beamforming methods detect two sources intermittently, while CLEAN continuously resolves three sources.

Furthermore, the frequency band of processing can highlight different sources, which is illustrated in Fig. 9. Fig. 9 shows that the microbaroms from the Atlantic Ocean have a lower centre frequency than those of the Mediterranean Sea. The Atlantic Ocean microbaroms are most coherent to the north–west in the frequency range of 0.1–0.3 Hz, those from the Mediterranean Sea appear from the east between 0.3–0.6 Hz. This is consistent with the earlier analysis by Assink *et al.* (2014).

Microbarom source regions are identified by cross-bearing localization, in which the detections at multiple IMS arrays are combined. In this procedure, it is assumed that there is an atmospheric duct in all directions, and that the propagation of microbarom signals is not strongly influenced by cross-winds or other along-path meteorological conditions (Smets & Evers 2014). The source locations are compared with microbarom source regions that have been predicted using the microbarom source model described by (Waxler *et al.* 2007), following the implementation described in Smets (2018). As an input for this model, the two-dimensional wave spectra (2DFD) obtained from the European Centre for Medium-Range Weather Forcast (ECMWF) deterministic high-resolution ocean wave model Cycle 36r1 (HRES-WAM) analysis (ECMWF 2008, 2016) have been used.

Figs 10(a) and (b) show the results of this approach for the frequency ranges of 0.1–0.3 and 0.3–0.6 Hz. For both frequency bands CLEAN resolved several subdominant sources, which could have been missed when applying conventional beamforming methods. Because of this, the same microbarom sources are resolved at different IMS stations, resulting in better microbarom source localization based on IMS observations. In case of the lower frequency band more microbarom sources are resolved in the region of the Atlantic ocean, the higher frequency band highlights two sources towards the Mediterranean sea. For both ranges of frequency, the resolved microbarom source regions are in a particularly good agreement with the microbarom prediction model.

5 DISCUSSION AND CONCLUSION

In this study, a CLEAN array processing algorithm is presented that has been inspired by earlier work (Sijtsma 2007; Gal *et al.* 2016). CLEAN is a post-processing method that can be applied to conventional beamform techniques, such as Bartlett and Capon. Because contributions to the total *f*/*k* spectrum are iteratively removed in this procedure, subdominant sources can be identified. Moreover, a more peaked *f*/*k* spectrum is obtained because the array response is deconvolved in the process. The performance of CLEAN is found to be dependent on the beamform resolution, which is in line with earlier work by Gal *et al.* (2016).

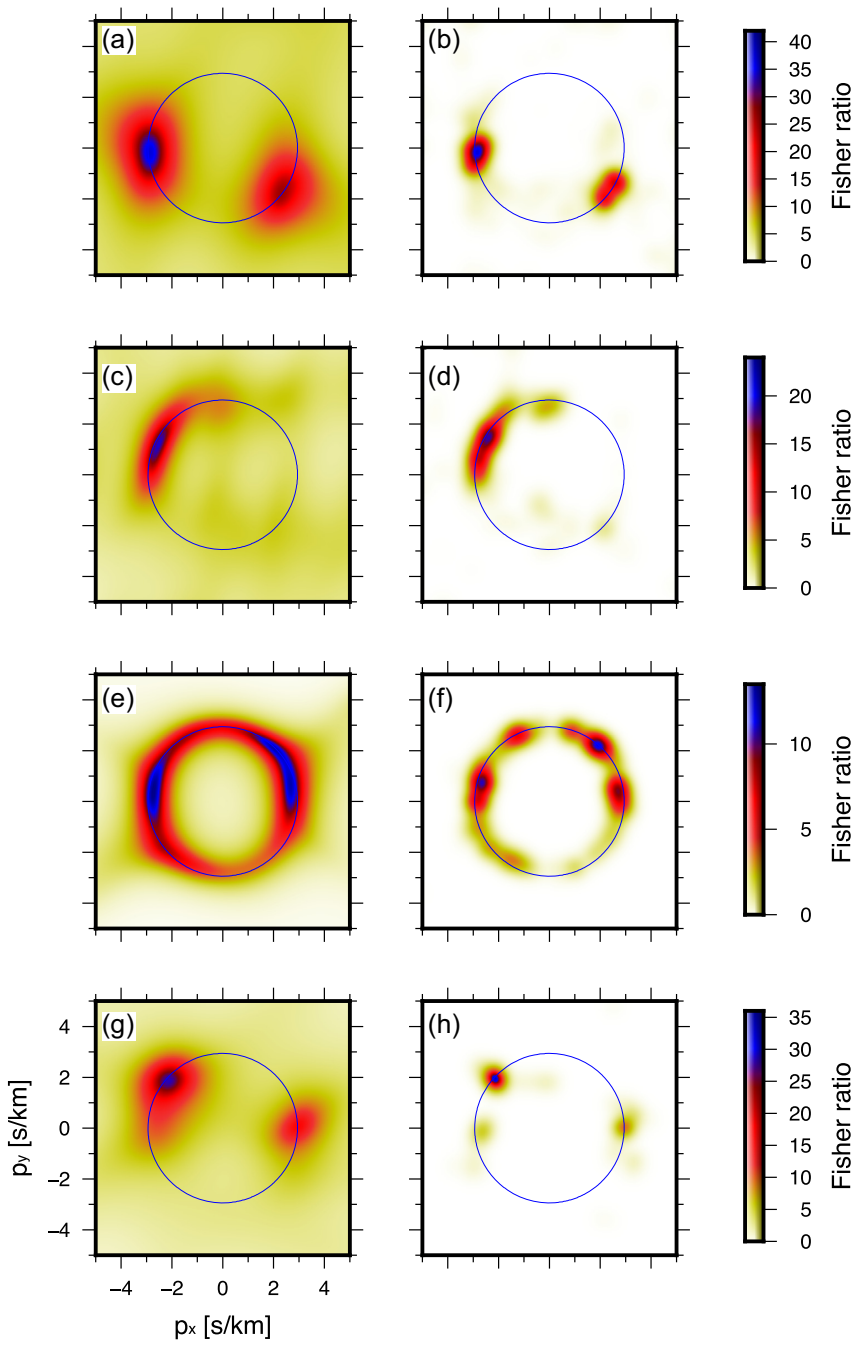

Figure 7. The *f*/*k* spectra of IS18 (a and b), IS26 (c and d), IS42 (e and f) and IS48 (g and h) before and after CLEAN, between 0.1 and 0.3 Hz for the first 2000 s of data on 2011 January 17. The blue ring indicates the speed of sound at standard sea level (15 °C and 1.225 kg m^{-3}), $c_{\text{app}} = 340$ m s^{-1}.

Moreover, the use of Fisher statistics for signal detection and the determination of a CLEAN stopping criterion is proposed. This stopping criterion has been identified in earlier work as a critical parameter for the performance of CLEAN (Clark 1980; Sijtsma 2007; Gal *et al.* 2016). The efficiency of the method is demonstrated using a Monte Carlo simulation with uniform Gaussian white noise. From this test, it can be concluded that the central F-distribution can be used as guidance to estimate a CLEAN stopping criterion. The probability of false alarms can be estimated when it is assumed that the remainder of the cross-spectral density matrix consists of (incoherent) white noise after beamform iterations.

Furthermore, synthetic tests have been performed to simulate the detectability of multiple continuous infrasound sources surrounding an array. The tests show that the backazimuth and the apparent velocity are accurately resolved. Based on this, it is concluded that that the PSF in combination with the two standard deviations distribution is adequate for distinguishing multiple sources. The Capon method has been found to provide more accurate results when compared to the Bartlett method, which is related to the higher spectral resolution of the former method.

It has been shown that the properties of Fisher statistics can be used to discriminate between coherent and incoherent signals. As a

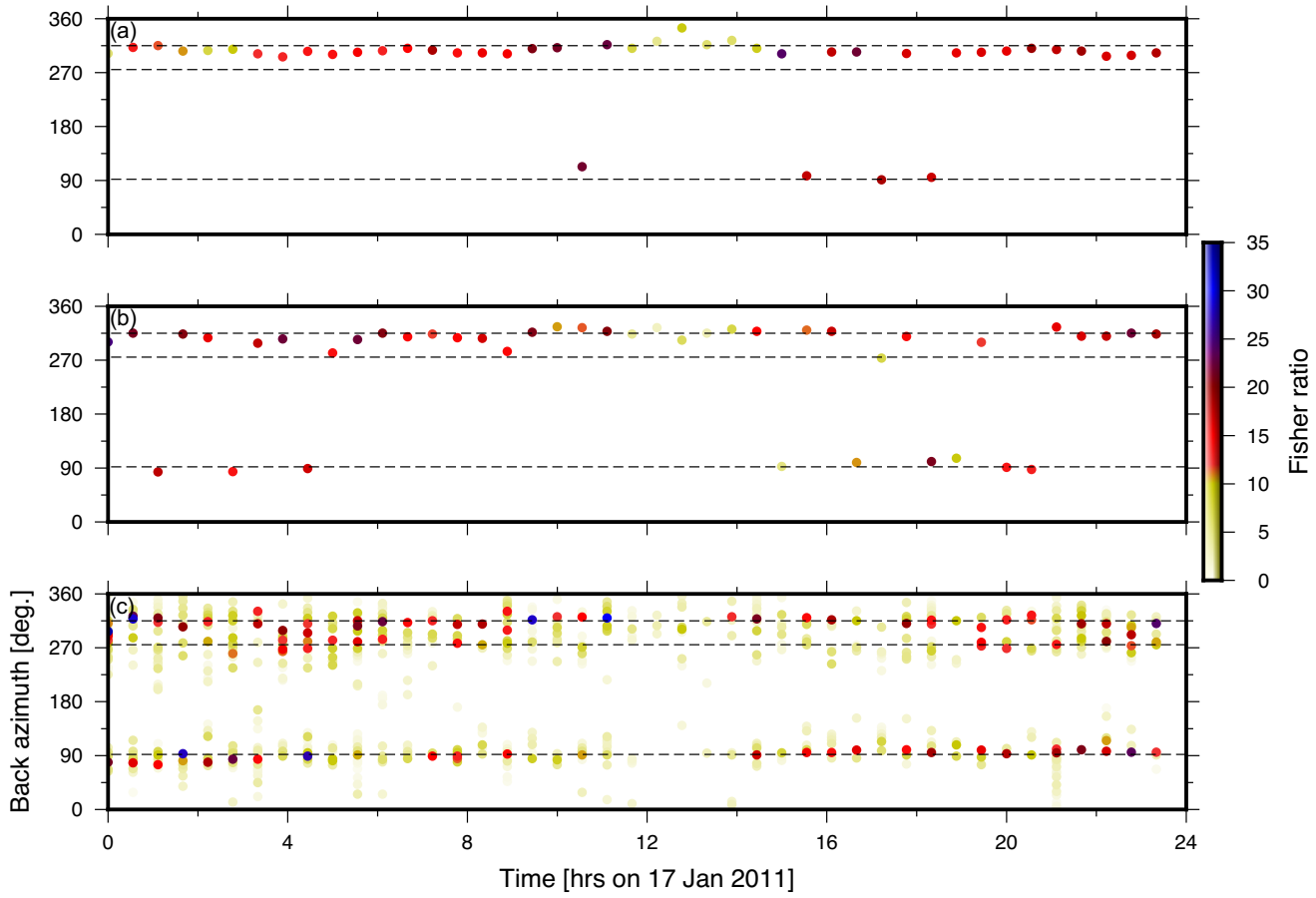

Figure 8. Infrasound detections on 17 January 2011 in the 0.1–0.3 Hz frequency band. Panel (a) shows the maximum contribution of the Bartlett *f*/*k* spectrum without CLEAN. (b) The maximum contribution of the Capon *f*/*k* spectrum without CLEAN and panel (c) reveals the outcome after application of the proposed CLEAN algorithm on the Capon *f*/*k* spectra. The dotted lines indicate the mean backazimuths that are associated with the observed microbaroms throughout the day. The dots are coloured coded by the Fisher ratio.

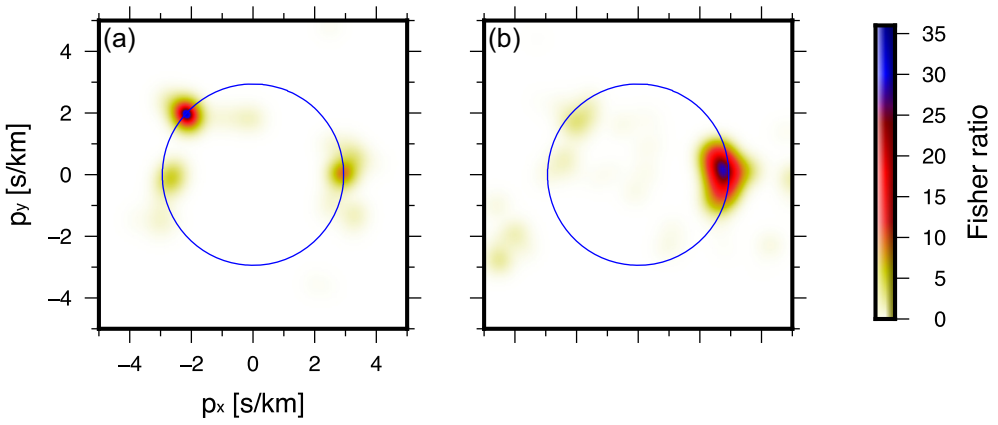

Figure 9. CLEAN *f*/*k* spectra of IS48 between (a) 0.1–0.3 Hz and (b) 0.3–0.6 Hz for the first 2000 s of data on 2011 January 17.

result, the Fisher ratio shall be used as the CLEAN stopping criterion. Nonetheless, in the estimation of SNR levels, it has been found that the resolved Fisher ratio is not always in agreement with the theoretical value that would be expected from the SNR conditions and the degrees of freedom in the data set. The bias is attributed to the fact that the noise cannot longer be considered as uncorrelated Gaussian white noise when multiple coherent signals are present in the array recordings. Further research is needed to understand the noted bias between the theoretical and the resolved Fisher ratio, in the case of multiple sources. This is further elaborated on in Appendix S1.

CLEAN has been applied to infrasound data recorded on multiple IMS arrays that are located around the Northern Atlantic. The results show that multiple microbarom sources can be resolved,

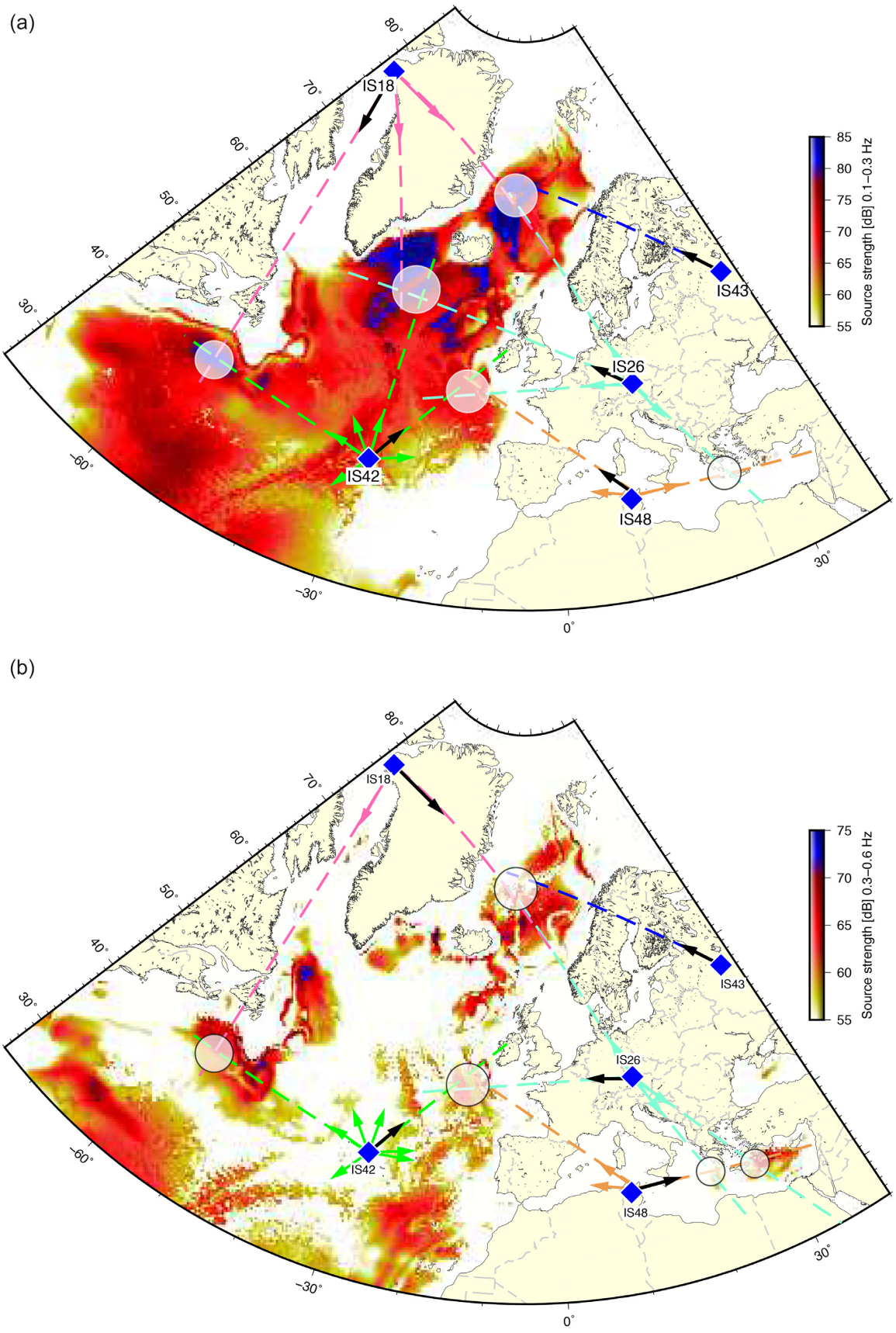

Figure 10. Microbarom source region predictions for frequencies between 0.1 and 0.3 Hz (a) and between 0.3 and 0.6 Hz (b) from 2011 January 17 00:00 UTC till 00:30 UTC (Waxler & Gilbert 2006; Smets 2018). IS48, IS42, IS26, IS43 and IS18 are indicated by blue diamonds. Backazimuth projections of all resolved sources are indicated by solid arrows (Fig. 7), the black solid arrow indicates the dominant source. Transparent circles indicate possible source locations found by cross-bearing.

including regions that would have been obscured if conventional processing methods would have been used. Microbarom source locations are obtained by cross-bearing localization and are in agreement with simulated microbarom source regions. It should be noted that the effects of propagation conditions are neglected in the current approach which, in combination with the dynamic nature of the microbaroms, explain some variation in backazimuth with time. Such effects could be accounted for by back projecting using a ray theoretical approach (Smets & Evers 2014).

Although the use of CLEAN beamforming allows for the detection of concurrent sources around an infrasound array, the method is computationally expensive compared to methods in which only the dominant source is to be detected. Moreover, the performance of CLEAN depends on the setting of various parameters that require careful tuning. This includes the choice of the beamforming weights and the setting of the ϕ value, the percentage of source removal per iteration. The setting of ϕ depends on the combination of array layout, processing frequency and the SNR. Therefore, it is important to analyse the sensitivity of the beamforming results to the choice of processing parameters.

Conventional beamforming algorithms can only confidently detect the most dominant source in each processing window and cannot confidently distinguish other concurrent sources from side lobes. The CLEAN implementation by Gal *et al.* (2016) iteratively resolves more sources. However, without a statistical framework, the number of iterations, which is pre-defined, is arbitrary and there is no certainty in the process with regard to true or false sources. In the presented implementation, a Fisher statistics framework is used to define a stopping criterion so that there is statistical certainty that the resolved sources are real. In the case of IS42 the initial *f*/*k* spectrum is 'smeared' over almost 360°. This is because IS42 is located on an island with sources all around it, including perhaps local and weaker sources that are not resolved in the microbarom model. The model averages microbarom source activity over a period of 6 hr. Therefore sources that are active for only a small fraction of that period are suppressed. However, a processing window of 2000 s with CLEAN can resolve such local, short duration sources. Additionally, IS42 is located relatively close to North-Atlantic microbarom source regions highlighted in the model (Fig. 10). Thus, it can separate the source region into more subsources that are two standard deviations apart in the *f*/*k* spectrum.

Previous studies have discussed other beamforming algorithms to identify multiple sources within the same frequency band (e.g. MUSIC; Schmidt 1986). den Ouden *et al.* (2018) compared the CLEAN and MUSIC algorithms, and discussed the benefits of CLEAN over MUSIC. CLEAN does not require source knowledge while the MUSIC algorithm needs the user to define the number of sources. If this number is incorrect, the outcome of the algorithm is incorrect. Furthermore, MUSIC can only resolve as many sources as array elements.

The enhanced beamforming resolution of CLEAN improves the capabilities of infrasound as a monitoring technique. This comes to the benefit of infrasonic monitoring of nuclear tests as well as natural hazards, such as volcanoes, earthquakes and hurricanes. In addition, high-resolution microbarom observations can be useful in the assessment of microbarom source models (Waxler *et al.* 2007) as well as in the remote sensing of the middle and upper atmosphere, for which microbarom signals have been used in previous research (Donn & Rind 1972; Smets 2018). Besides the application to infrasound arrays, the algorithm can be applied to improve on the limited *f*/*k* spectral resolution of arrays with a low number of elements, such as the IMS hydro-acoustic triplet arrays that are deployed in the world's oceans.

ACKNOWLEDGEMENTS

The authors thank the CTBTO and station operators for the high quality of IMS data and products. IMS data can be accessed through the vDEC (see https://www.ctbto.org/specials/vdec/). All figures have been created using Generic Mapping Tools (Wessel *et al.* 2013). OdO and JA are funded by a Human Frontier Science Program Young Investigator Grant (SeabirdSound - RGY0072/2017). The contributions of PS, SS-K and LE are funded through a VIDI project from the Netherlands Organisation for Scientific Research (NWO), Project 864.14.005. The contribution of GA is funded through the Marie Curie Action WAVES from the European Union within H2020, Grant Number 641943. The authors are grateful for helpful reviews by the Editor, David Green and David Fee.

REFERENCES

Assink, J., Waxler, R., Smets, P. & Evers, L., 2014. Bidirectional infrasonic ducts associated with sudden stratospheric warming events, *J. geophys. Res. Atmos.,* **119**(3), 1140–1153.

Bartlett, M., 1948. Smoothing periodograms from time-series with continuous spectra, *Nature,* **161**(4096), 686.

Billingsley, J. & Kinns, R., 1976. The acoustic telescope, *J. Sound Vib.,* **48**(4), 485–510.

Campus, P. & Christie, D., 2010. Worldwide observations of infrasonic waves, in *Infrasound Monitoring for Atmospheric Studies,* pp. 185–234, eds Le Pichon, A., Blanc, E. & Hauchecorne, A., Springer.

Capon, J., 1969. High-resolution frequency-wavenumber spectrum analysis, *Proc. IEEE,* **57**(8), 1408–1418.

Clark, B., 1980. An efficient implementation of the algorithm 'CLEAN', *Astron. Astrophys.,* **89,** 377–378.

den Ouden, O., Assink, J., Smets, P. & Evers, L., 2018. Well-founded parameters for CLEAN and MUSIC beamforming, in *EGU General Assembly Conference Abstracts,* Vol. 20, p. 13594.

Donn, W. & Rind, D., 1972. Microbaroms and the temperature and wind of the upper atmosphere, *J. Atmos. Sci.,* **29**(1), 156–172.

ECMWF, 2008. Part vii: ECMWF wave model, IFS documentation-Cy33r1, Tech. rep., The European Centre for Medium-Range Weather Forecast, Reading, United Kingdom.

ECMWF, 2016. Changes in ECMWF model, Tech. rep., The European Centre for Medium-Range Weather Forecast, Reading, United Kingdom.

Edwards, W.N. & Green, D.N., 2012. Effect of interarray elevation differences on infrasound beamforming, *Geophys. J. Int.,* **190**(1), 335–346.

Evers, L.G., 2008. *The inaudible symphony: on the detection and source identification of atmospheric infrasound, PhD thesis,* TU Delft, Delft University of Technology.

Fisher, R., 1948. *Statistical Methods for Research Workers,* Hafner.

Gal, M., Reading, A., Ellingsen, S., Koper, K., Burlacu, R. & Gibbons, S., 2016. Deconvolution enhanced direction of arrival estimation using one-and three-component seismic arrays applied to ocean induced microseisms, *Geophys. J. Int.,* **206**(1), 345–359.

Garrett, M.A., 2013. Radio astronomy transformed: aperture arrays—past, present and future, in *2013 Africon,* pp. 1–5, IEEE, Pointe-Aux-Piments, Mauritius.

Harjes, H. & Henger, M., 1973. Array-seismologie, *Z. Geophys.,* **39,** 865–905.

Högbom, J., 1974. Aperture synthesis with a non-regular distribution of interferometer baselines, *Astron. Astrophys. Suppl. Ser.,* **15,** 417.

Husebye, E. & Ruud, B., 1989. Array seismology–past, present and future developments, in *Observatory Seismology,* pp. 123–153, ed. Litehiser, J.J., University of California Press.

Jansky, K.G., 1932. Directional studies of atmospherics at high frequencies, *Proc. Inst. Radio Eng.,* **20**(12), 1920–1932.

Melton, B.S. & Bailey, L.F., 1957. Multiple signal correlators, *Geophysics,* **22**(3), 565–588.
Michel, U. *et al.*, 2006. History of acoustic beamforming, in *Berlin Beamforming Conference,* Berlin, Germany, pp. 21–22.
Rost, S. & Thomas, C., 2002. Array seismology: Methods and applications, *Reviews of geophysics,* **40**(3), 2–1-2-27.
Schmidt, R., 1986. Multiple emitter location and signal parameter estimation, *IEEE Trans. Antennas Propag.,* **34**(3), 276–280.
Schweitzer, J., Fyen, J., Mykkeltveit, S., Kværna, T. & Bormann, P., 2002. Seismic arrays , Bormann, P., in *New Manual of Seismological Observatory Practice, p. 52,* IASPEI.
Shumway, R.H., 1971. On detecting a signal in N stationarily correlated noise series, *Technometrics,* **13**(3), 499–519.
Sijtsma, P., 2007. Clean based on spatial source coherence, *Int. J. Aeroacoust.,* **6**(4), 357–374.
Smart, E. & Flinn, E.A., 1971. Fast frequency-wavenumber analysis and Fisher signal detection in real-time infrasonic array data processing, *Geophys. J. Int.,* **26**(1-4), 279–284.
Smets, P., 2018. Infrasound and the dynamical stratosphere: a new application for operational weather and climate prediction, *Doctoral thesis*, Delft University of Technology.
Smets, P. & Evers, L., 2014. The life cycle of a sudden stratospheric warming from infrasonic ambient noise observations, *J. geophys. Res. Atmos.,* **119**(21), 12–084.
Smink, M., Assink, J., Evers, L., Bosveld, F. & Smets, P., 2018. A 3D array for analysis of regional infrasound propagation in the atmospheric boundary layer, in *EGU General Assembly Conference Abstracts, Vol. 20,* p. 6871.
Sutherland, L.C. & Bass, H.E., 2004. Atmospheric absorption in the atmosphere up to 160 km, *J. acoust. Soc. Am.,* **115**(3), 1012–1032.
Viberg, M. & Krim, H., 1997. Two decades of array signal processing, in *Proceedings of the 31st Asilomar Conf. Sig., Syst., Comput.,* Pacific Grove, CA.
Waxler, R. & Assink, J., 2019. Propagation modeling through realistic atmosphere and benchmarking, in *Infrasound Monitoring for Atmospheric Studies,* pp. 509–549, eds Le Pichon, A., Blanc, E. & Hauchecorne, A., Springer.
Waxler, R. & Gilbert, K.E., 2006. The radiation of atmospheric microbaroms by ocean waves, *J. acoust. Soc. Am.,* **119**(5), 2651–2664.
Waxler, R., Gilbert, K., Talmadge, C. & Hetzer, C., 2007. The effects of finite depth of the ocean on microbarom signals, in *8th International Conference on Theoretical and Computational Acoustics (ICTCA),* Crete, Greece.
Wessel, P., Smith, W.H., Scharroo, R., Luis, J. & Wobbe, F., 2013. Generic mapping tools: improved version released, *EOS, Trans. Am. geophys. Un.,* **94**(45), 409–410.

SUPPORTING INFORMATION

Supplementary data are available at *GJI* online.

Figure S1. The theoretical central and non-central F-distribution based on synthetic data set A (Table 1). The red curve indicates the central distribution, the grey curves the theoretical non-central distribution for each source. The dotted lines are the resolved mean Fisher ratios, while the orange histograms determine the outcome of the Monte Carlo runs. The observed differences between histograms and theoretical distributions can be explained by the coherence of the background noise.

Please note: Oxford University Press is not responsible for the content or functionality of any supporting materials supplied by the authors. Any queries (other than missing material) should be directed to the corresponding author for the paper.